



Please cite the Published Version

Gao, Z, Zhang, X, Kulczyk-Malecka, J , Chen, Y, Bousser, E, Kelly, P  and Xiao, P (2021) Ceramic buckling for determining the residual stress in thin films. Scripta Materialia, 201. ISSN 1359-6462

DOI: <https://doi.org/10.1016/j.scriptamat.2021.113949>

Publisher: Elsevier

Version: Accepted Version

Downloaded from: <https://e-space.mmu.ac.uk/627941/>

Usage rights:  [Creative Commons: Attribution-Noncommercial-No Derivative Works 4.0](#)

Additional Information: Author accepted manuscript accepted for publication in Scripta Materialia. Published by Elsevier and copyright Acta Materialia Inc.

Enquiries:

If you have questions about this document, contact openresearch@mmu.ac.uk. Please include the URL of the record in e-space. If you believe that your, or a third party's rights have been compromised through this document please see our Take Down policy (available from <https://www.mmu.ac.uk/library/using-the-library/policies-and-guidelines>)

Ceramic buckling for determining the residual stress in thin films

Zhaohe Gao^{a*}, Xun Zhanga, Justyna Kulczyk-Maleckab, Ying Chen^a, Etienne Bousser^{a,c}, Peter Kelly^b
and Ping Xiao^{a*}

^a*Henry Royce Institute, Department of Materials, University of Manchester, Manchester, M13 9PL, UK*

^b*Surface Engineering Group, Manchester Metropolitan University, Manchester, M1 5GD, UK*

^d*Department of Engineering Physics, Polytechnique Montréal, Montreal, Canada, H3T 1J4*

Abstract

A new technique for determination of residual stress in thin films and coatings has been presented. The method consists of focused ion beam milling to create a lamella of thin film, followed by analysis of stress driven buckling profile of undercut lamella (beam) to extract residual stress. The residual stresses in crystalline TiN and Al₂O₃ films, produced by reactive magnetron sputtering and thermal oxidation, respectively, have been successfully determined by this new technique and validated by conventional X-ray diffraction and photoluminescence piezospectroscopy techniques, respectively. This new technique successfully measures and tracks the evolution of residual stress in as-deposited and different thermally cycled amorphous SiAlN films induced by thermal mismatch or relieved via mechanical twinning in interlayer, where diffraction methods are not applicable, thereby evaluating the thermal cycling performance of amorphous SiAlN coatings for protection of Ti at high temperature.

Keywords: Ceramic Buckling; Residual Stress; Focused ion beam; Films and Coatings; Amorphous.

Thin films and coatings, e.g. nitrides, oxides, etc., have been widely used in many applications, such as semiconductors, optical devices, cutting tools, medical implants and thermal barrier coating systems [1-6]. Residual stress, derived from non-equilibrium growth, thermal expansion mismatch, lattice mismatch and other factors, is almost unavoidable in such films and coatings [7-10]. The residual stress can significantly affect both the functional e.g. capacitance, conductivity, etc., and mechanical performance, e.g. adhesion, fracture, etc., of these films and coatings [11-15]. Therefore, measurement of the residual stress is of crucial importance for materials design and determination of in-service performance of these films and coatings. Due to the reduced geometry of the thin films and coatings, their residual stresses are generally measured by diffraction methods (e.g. X-ray or neutron diffraction)[16-19]. However, the diffraction methods are restricted to crystalline materials and not applicable to amorphous materials and the low spatial resolution of most diffraction methods prevents the measurements of site-specific local stresses [19]. The evaluation of local residual stress and the residual stress in amorphous thin coatings has been made possible by the development of the Focused Ion Beam-Digital Image Correction (FIB-DIC) technique [17, 20-22]. In these methods, a FIB is used to mill an incremental trench and the gradual strain relief due to progressive milling can be acquired by means of DIC analysis of scanning electron microscopy images. However, the calculation of the residual stress usually needs complex simulation and modelling [20].

In this study, we present a new and relatively simpler technique for determining the site-specific local residual stress in thin films, especially amorphous films. The technique involves FIB milling to create a lamella of the thin coating and analysis of the stress-driven deflection (buckling) profile of the lamella to directly extract the residual stress based on beam theory. To validate such technique, the residual stresses in crystalline TiN and Al₂O₃ films have been determined by this new technique, and agree with values measured by a couple of well-established conventional techniques. Then this technique has been used to track the evolution of residual stress in an amorphous SiAlN sputtered coating induced by thermal treatment.

Three ceramic coatings, SiAlN on pure Ti plate, TiN on Si wafer, and Al₂O₃ formed on oxidised FeCrAlY alloy plate, were prepared in this work. The SiAlN coating with a thickness of 1.2 μ m was deposited on pure Ti by reactive magnetron sputtering, while a 300 nm thick Mo layer

was deposited as an interlayer between the SiAlN coating and Ti substrate. Deposition of this coating was carried out in a Teer Coatings UDP 350 magnetron sputtering system, illustrated elsewhere [23]. Three vertically opposed unbalanced magnetrons ($300 \times 100 \text{ mm}^2$) were mounted through the sputtering rig walls enclosing a rotating substrate unheated holder placed in the middle of the chamber. The commercially pure Si, Al, and Mo (interlayer deposition) targets were attached to the magnetrons. The chamber was pump down to a base pressure of below $1 \times 10^{-3} \text{ Pa}$ before the coatings' deposition. Prior to deposition, the substrates were sputter cleaned for 15 minutes at a bias voltage of -600 V DC applied to the substrate holder. The Si, Al, and Mo targets were powered by Advanced Energy Pinnacle Plus power supplies operating in pulsed DC mode at a pulse frequency of 100 kHz (duty cycle = 60%). Simultaneously, a bias of -30 V was applied to the substrate holder throughout coating deposition to ensure the coatings were well adhered to the substrate. The argon to nitrogen gas ratio during the reactive sputter deposition of the nitride layer was controlled using an optical emission monitoring (OEM) system and mass flow controllers (MKS Ltd.) were used to introduce the appropriate amount of gases to the sputtering chamber. The TiN coating with a thickness of $5.8 \text{ }\mu\text{m}$ was deposited on a Si wafer substrate by pulsed-DC magnetron sputtering. The two-inch Ti target was powered by Advanced Energy Pinnacle Plus power supply running in pulsed DC mode at a pulse frequency of 300 kHz (duty cycle = 88%) and a bias of -100 V was applied to the substrate during coating deposition. The Al_2O_3 scale with a thickness of $1.3 \text{ }\mu\text{m}$ was formed on a polished FeCrAlY alloy (Goodfellow, Fe 72.8%, Cr 22%, Al 5%, Y 0.1%, Zr 0.1%, wt) plate after oxidation. The alloy was oxidized at 1200°C in air for 2 h in a CMTM furnace with a heating rate of $100^\circ\text{C}/\text{minute}$ and followed by forced air cooling.

In order to determine the residual stresses in the above mentioned coating lamella milling was carried out using a focused ion beam (FIB, FEI, Quanta 3D and Helios 660 with 30 KV working voltage). All the three coatings, SiAlN, TiN and Al_2O_3 were assumed to have homogeneous microstructure and uniform thickness, and the studied positions were randomly selected. The process consisted of four following steps: 1) lamella preparation; 2) undercut of lamella; 3) acquire the buckled lamella image; 4) fitting of the buckled beam and stress calculation, as illustrated in Fig.1. Firstly, a lamella containing both the substrate and the coating was created (tilting angle 52°) by milling two symmetric trenches from the surface with a beam current ranging from 7 nA to 1 nA (Fig.1 a). The dimension of the lamellas could

vary from 10 μm to 17 μm in length (X axis), 0.4 μm to 1 μm in thickness (Z axis) and 3-6 μm in height (depth, Y axis), as shown in Fig.1 a. The lamella was then undercut (tilting angle 0°) to remove the substrate material and/ or the bottom part of coating material to provide a clear image of the buckling of the lamella. The milling current ranges from 0.3 nA to 1 nA (Fig.1 b) depending on the materials and the thickness of the lamella. The compressive residual stress within the lamella caused buckling of the beam once the undercut was finished (Fig. 1 c), as also shown in Supplementary video 1 and 2 in detail. The buckled beam was imaged by SEM and the buckling profile was determined from the image, illustrated elsewhere [24].

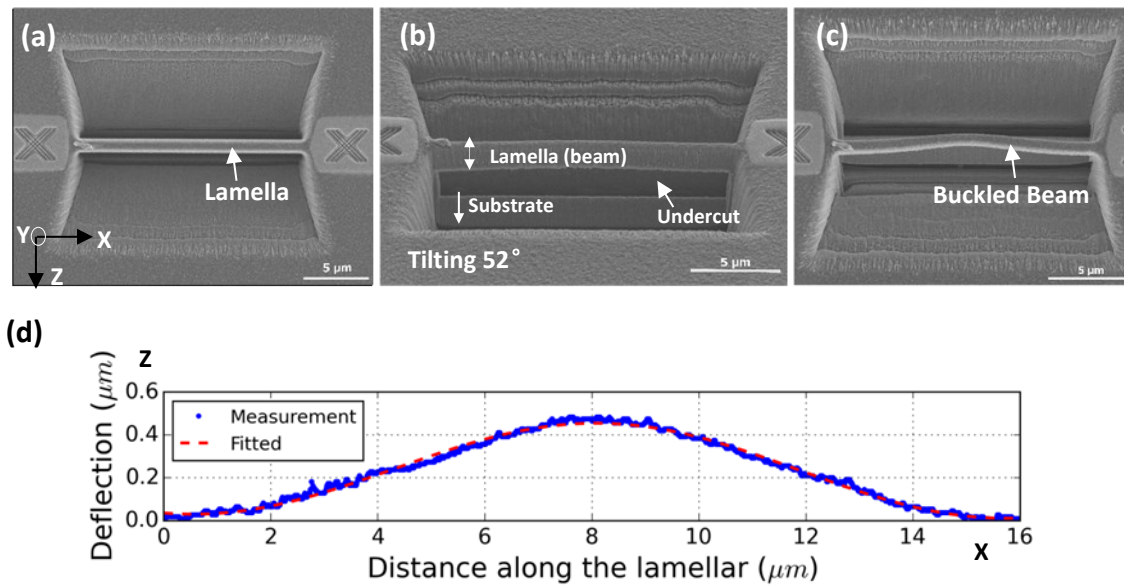


Fig.1 Schematic diagrams of FIB milling-stress driven buckling technique. (a) Lamella preparation by FIB; (b) Undercut of lamella (beam); (c) Buckled beam; (d) Fitting the deflection of beam and stress calculation.

The stress was calculated based on the elementary beam theory assuming the deformation is purely elastic (this will be justified later) and the stress is uniform through the thickness of the coating. The buckling profile of the coating can be described by a cosine function, W , given by [25]:

$$W = C[\cos(F * x) - 1] \quad (1)$$

C is obtained by fitting the buckling profile. The strain parallel to the lamella is linked to C through equations (2-4)

$$C = \frac{2}{\sqrt{1+4\pi^2 F_1}} \sqrt{\frac{\lambda}{4\pi^2} (1 + 4\pi^2 F_1) - 1} \quad (2)$$

$$F_1 = \frac{EI}{A_{xz}l^2} \quad (3)$$

$$A_{xz} = k_s \frac{EA}{2(1+\nu)} \quad (4)$$

Where k_s is the Timoshenko shear coefficient, which depends on the geometry; normally $k_s = 5/6$ for a rectangular section; l : length of the lamella; I : moment of inertia; A : area of the cross-section; E : elastic modulus; ν : Poisson's ratio.

Once λ has been obtained, then the strain, ε , parallel to the interface can be obtained based on the equation (5):

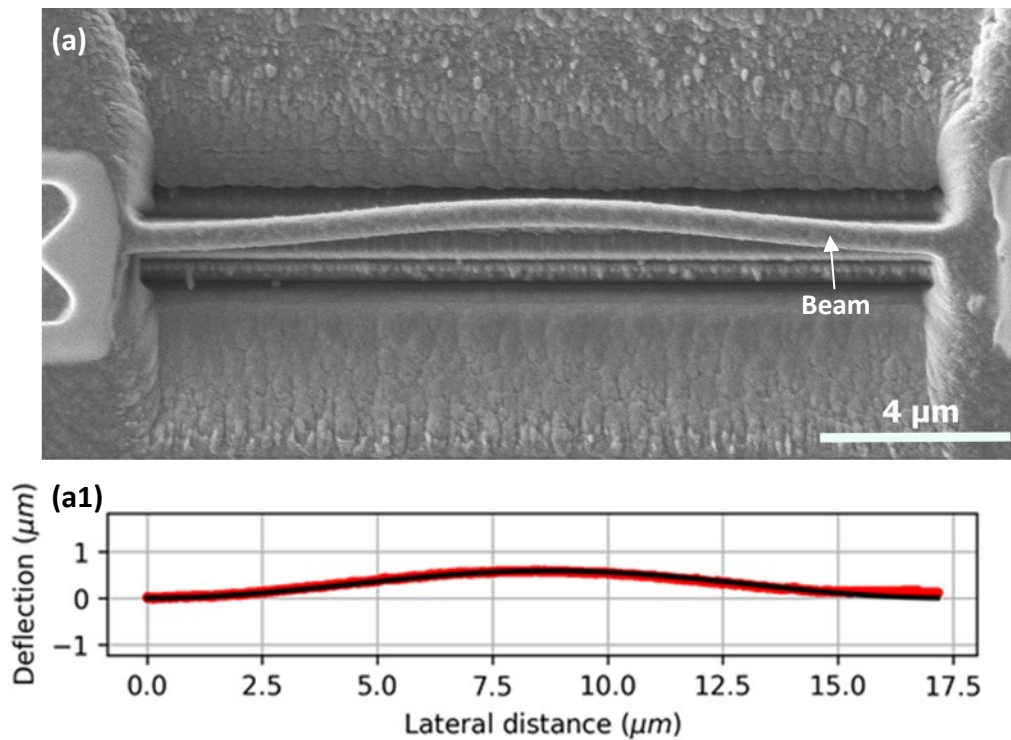
$$\lambda = 12 \left(\frac{l}{h} \right)^2 \varepsilon \quad (5)$$

For each coating, at least three lamellas were prepared and analysed.

In order to validate the stress measured by the proposed method, the stress in the as-deposited TiN coating was also measured by the conventional XRD $\sin^2\psi$ method using a Bruker D8 Discover X-ray diffractometer. An incident beam angle of 5° was used during the measurement. The diffraction peaks for all the measurement were acquired from the (420) plane of TiN using Co K α radiation ($\lambda_{Co} = 1.78897\text{\AA}$), described in detail elsewhere [6, 23]. The stress in the crystalline Al_2O_3 scale on oxidised FeCrAl alloy was measured using photoluminescence piezospectroscopy (PLPS) on a Raman microscope 1000 (Renishaw™, Gloucestershire, UK) equipped in an argon laser source ($\lambda = 514\text{ nm}$), described in detail elsewhere [26]. More details on the measurements are given in the supplementary material.

The compressive residual stress within the beam causes the buckling of the coating beam once the lamella (beam) has been undercut to remove the substrate material and/ or the bottom part of coating material to make a clear buckling of lamella. Fig. 2 a shows a buckled beam from the TiN coating after the FIB undercut. Such buckling is fully elastic deformation, as the beam returns to its unbent condition once one side of the beam is cut off, as shown in Supplementary video 1. The residual stress in the TiN calculated from the buckling profile is $-1.63 \pm 0.27\text{ GPa}$, which is in reasonable agreement with the value $(-1.250 \pm 0.33\text{ GPa})$ measured by the XRD $\sin^2\psi$ method, as shown in the Supplementary Material. The difference may arise from the uncertainty in the fitting process of the deflected beams and/ or the measurement of beam geometry. Fig. 2b shows a buckled beam of Al_2O_3 scale formed on the

oxidised FeCrAlY alloy after FIB undercut. Due to the high thermal mismatch between the FeCrAlY substrate and the Al_2O_3 scale, high compressive stress can build up in the Al_2O_3 scale after fast cooling [27]. The residual stress in the Al_2O_3 scale calculated on the buckling profile is -5.67 ± 0.46 GPa, which is slightly higher than the value (-4.73 ± 0.55 GPa) measured by PLPS, as shown in Supplementary Material. In this case, such a discrepancy may come from the slightly wrinkled surface of the Al_2O_3 scale and the variation in stress from place to place over the scale. These two cases verify that the new FIB milling-stress driven buckling method is effective and reliable for the determination of residual stress in thin films and coatings. In addition, this new method is directly observable, and does not need complex image analysis or numerical modelling. Nevertheless, this method is limited to films subject to compressive residual stresses and not applicable to tensile residual stresses. Different geometries, e.g. different length or thickness, of the lamellas have also been tested and the results are consistent to some extent. For coatings with relatively low residual stresses, long and slender lamellas, e.g. length $\geq 15 \mu\text{m}$, thickness $\leq 0.5 \mu\text{m}$, height $\leq 0.5 \mu\text{m}$, are desirable to get clear buckling for the coatings. In summary, the principle of this new technique suggests that it can be used to measure the residual compressive stress in many thin films and coatings.



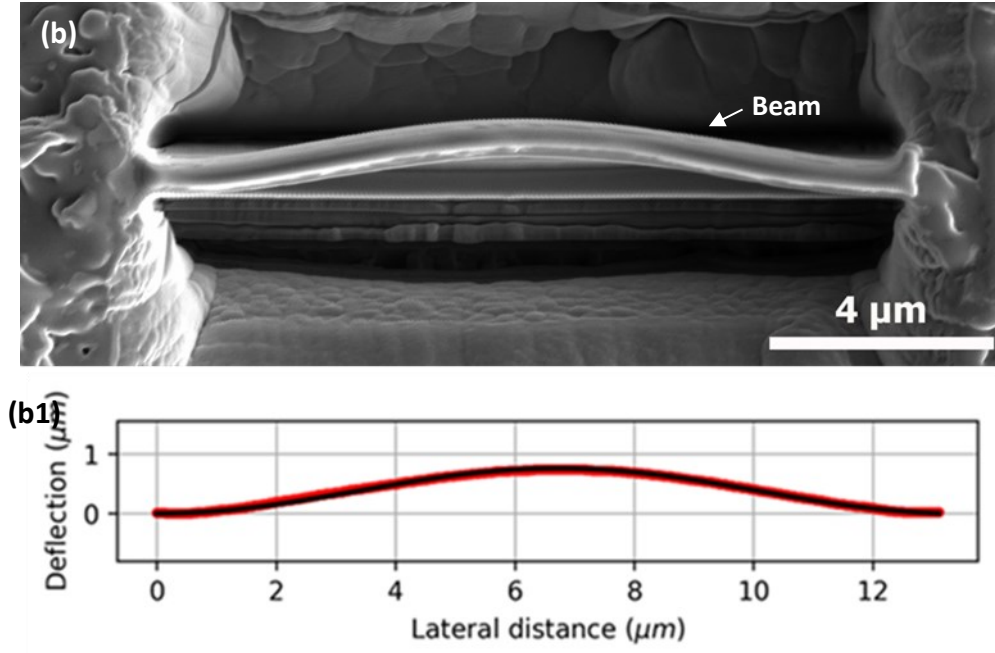
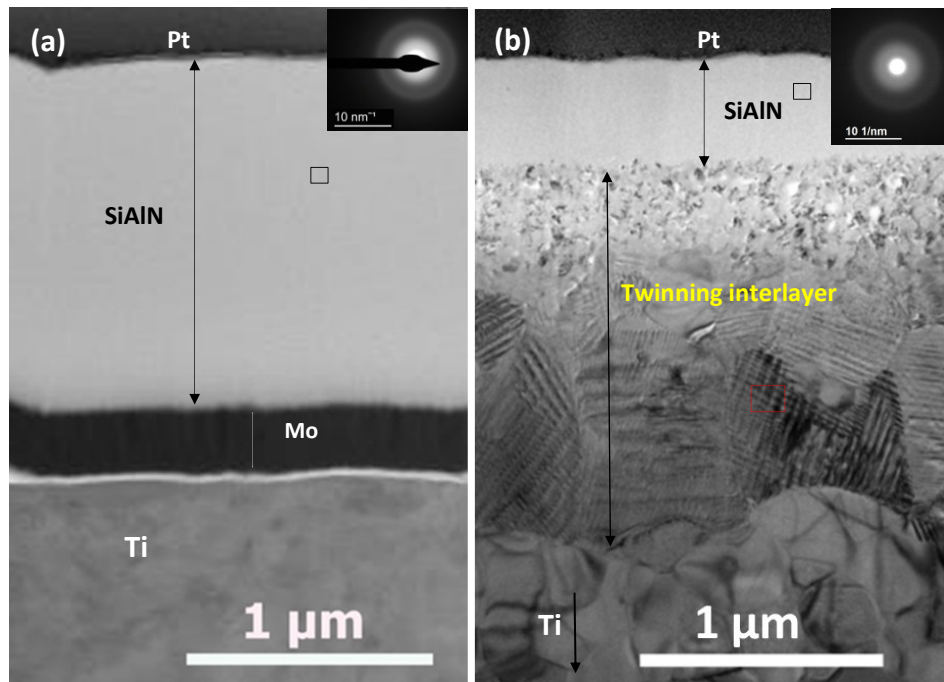


Fig. 2 (a) SEM image of a buckled beam of the TiN coating on a Si substrate; (a1) Fitting of the buckling profile of the beam; (b) SEM image of a buckled beam of Al₂O₃ scale on a FeCrAlY alloy; (b1) Fitting of the buckling profile of the beam. (a

The residual stress in an amorphous SiAlN coating was determined by the new FIB milling-stress driven buckling method. Additionally, the new method can track the evolution of residual stress in the amorphous SiAlN coating induced by thermal cycling treatment, thereby evaluating the thermal cycling performance of the SiAlN coatings. Amorphous SiAlN coatings with a Mo interlayer were deposited on pure Ti, as shown in Fig. 3 a and inset, and were thermally exposed at 800°C in air under different cycles. After 20 thermal cycles (100 h), interfacial interdiffusion and reaction between the SiAlN/Mo layers and the Ti substrate cause the formation of TiN_{0.26} deformation twins in the interlayer, as shown in Fig. 3 b and c, more details are shown in our previous work [28]. For the as-deposited SiAlN coating, the residual stress due to the coating-to-substrate thermal mismatch (SiAlN: 3.2 μm/(m·K), Ti: 8.6 μm/(m·K) [29, 30]) after the magnetron sputtering process is -1.82 ± 0.19 GPa calculated based on the buckling profile, as shown in Fig. 4 a. After one thermal cycle exposure, the residual stress increases from this as-deposited value, -1.82 GPa to -2.81 ± 0.26 GPa. The deflection of the beam after one thermal cycle is quite obvious, as shown in Fig. 4 b. Such an increase is believed to mainly derive from the thermal mismatch as the temperature increases from the deposition temperature of ~300-400°C to 800°C. It is essential to alleviate or even

avoid such stress/strains, as a relatively high stress could cause coating cracking and spallation. However, after 20 cycles (100 h), the SiAlN coatings have not undergone spallation or cracking (Fig. 3 b), which indicates excellent thermal cycling performance. Noticeably, the residual stress in the remnant amorphous SiAlN coating has reduced from -2.81 GPa after one cycle to -2.27 ± 0.3 GPa after 20 cycles, calculated based on the buckling profile, as shown in Fig. 4 c. The reduction of residual stress can be expected to explain the excellent thermal cycling performance of the amorphous SiAlN coatings. The $\text{TiN}_{0.26}$ interlayer is expected to accommodate the thermal mismatch strain between the SiAlN coating and substrate via mechanical twinning, and thereby effectively prolongs the cyclic lifetime. In conclusion, the FIB milling-stress driven buckling method can effectively track the change in residual stress in an amorphous coating induced by thermal mismatch or twinning relief, thereby evaluating the performance of amorphous coatings.



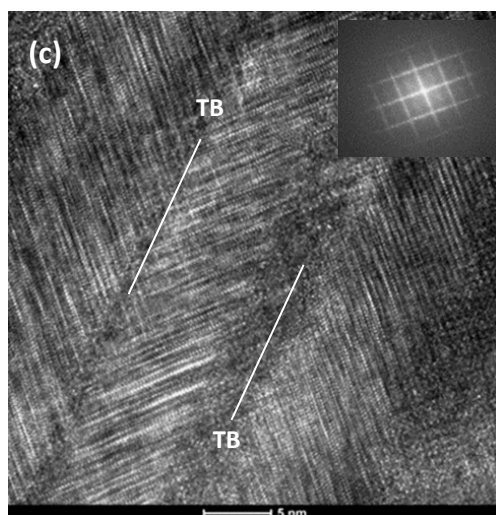
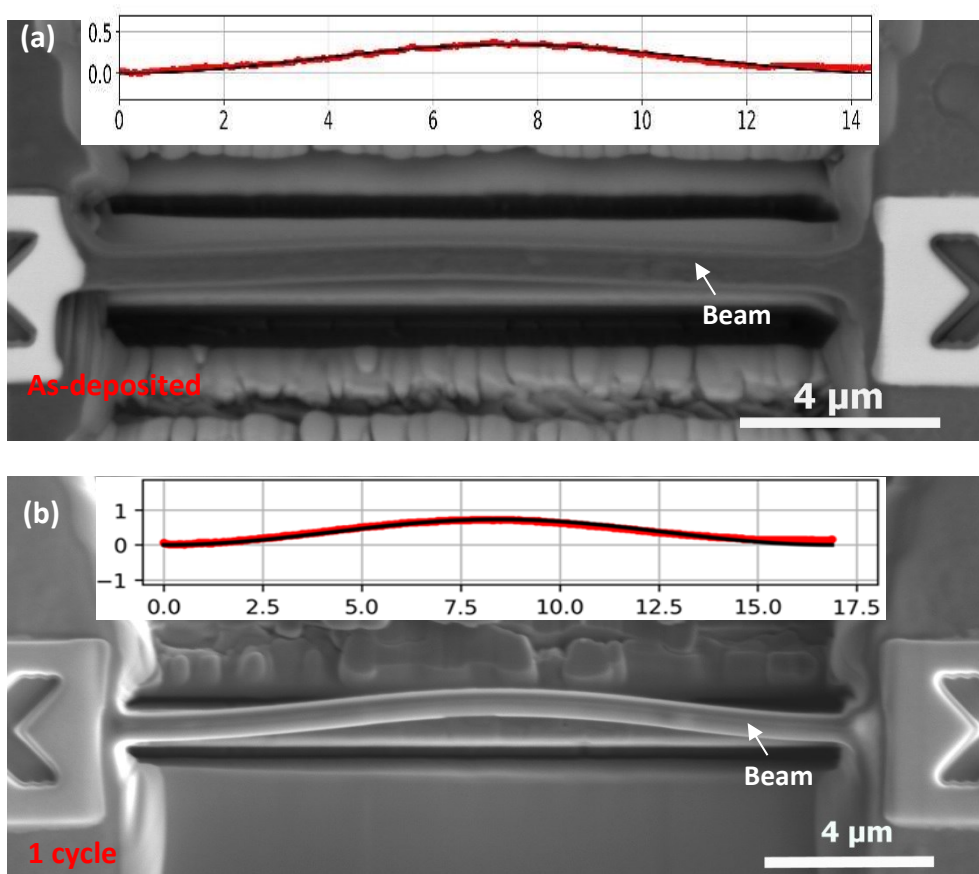


Fig. 3 (a) Cross-sectional STEM images of as-deposited SiAlN/Mo coating on Ti, inset shows diffraction pattern of the SiAlN coating; (b) Cross-sectional STEM images of SiAlN/Mo coating on Ti after annealing at 800°C in air for 20 cycles, inset shows diffraction pattern of the remnant SiAlN coating; (c) A HRTEM image with the incident beam along $[1-210]$ zone axis from the red framed region in (b) with an inset showing the corresponding Fast Fourier Transform (FFT), and twin boundary (TB) is marked.



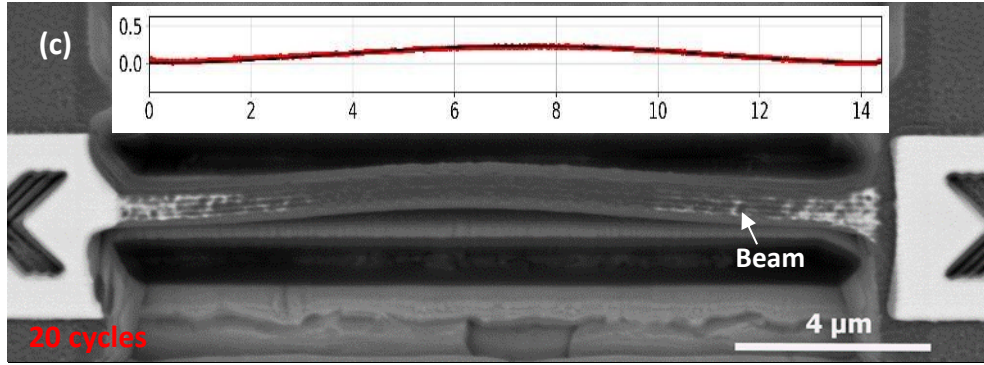


Fig. 4 (a) SEM image of a buckled beam of as-deposited SiAlN/Mo coating on Ti, inset shows the fitting of the buckling profile of the beam; (b) SEM image of a buckled beam of SiAlN/Mo coating on Ti after annealing at 800°C in air for 1 cycle, inset shows fitting of the buckling profile of the beam; (c) SEM image of a buckled beam of SiAlN/Mo coating on Ti after annealing at 800°C in air for 20 cycles, inset shows fitting of the buckling profile of the beam.

In conclusion, we present a new technique for determining compressive residual stresses in thin films and coatings. Two case studies on crystalline thin ceramic coatings (TiN and Al_2O_3) have been conducted, which after comparison with conventional measurements serve to validate the accuracy and reliability of this new technique. This new method is effective, relatively simple, and directly observable, and does not required complex image analysis or numerical modelling of FIB-DIC. The principle of this new technique suggests that it can be used to measure the residual stress in many thin films, including amorphous films. More broadly, it can be potentially used to measure the residual compressive stress of metallic or polymeric coatings and bulk materials, and even a few nanometres ultra-thin films potentially. The obtained residual stress is strongly related with the lifetime of the coating when coating failure occurs via buckling-driven delamination. Future work will focus on evaluating the coating's integrity by combining a more localised stress state determination for crack nucleation with the overall residual stress state determined in this work.

Acknowledgment

The authors would like to thank Mr. Gary Harrison and Dr. John Warren for the kind help on the X-ray diffraction experiments. PX would like to acknowledge support from Royal Academy of Engineering and Rolls-Royce for appointment of Rolls-Royce/Royal Academy of Engineering Research Chair in Advanced Coating Technology. The authors also thank Dr. Zhenbo Zhang for

his valuable discussion. Ying Chen would like to thank the new lecturer support from the Department of Materials at the University of Manchester. The authors are grateful for the Henry Royce Institute for Advanced Materials, funded through EPSRC grants EP/R00661X/1, EP/S019367/1, EP/P025021/1 and EP/P025498/1.

Reference

1. Ji, W., et al., *Dip Coating Passivation of Crystalline Silicon by Lewis Acids*. ACS Nano, 2019. **13**(3): p. 3723-3729.
2. Zhang, Y., et al., *Thin Nacre-Biomimetic Coating with Super-Anticorrosion Performance*. ACS Nano, 2018. **12**(10): p. 10189-10200.
3. Vega, J., et al., *Experimental studies of the effect of Ti interlayers on the corrosion resistance of TiN PVD coatings by using electrochemical methods*. Corrosion Science, 2018. **133**: p. 240-250.
4. Husain, E., et al., *Marine corrosion protective coatings of hexagonal boron nitride thin films on stainless steel*. ACS Appl Mater Interfaces, 2013. **5**(10): p. 4129-35.
5. Pogrebniak, A.D., et al., *Antibacterial effect of Au implantation in ductile nanocomposite multilayer (TiAlSiY)N/CrN coatings*. ACS Appl Mater Interfaces, 2019.
6. Chen, Y., et al., *Characterization and understanding of residual stresses in a NiCoCrAlY bond coat for thermal barrier coating application*. Acta Materialia, 2015. **94**: p. 1-14.
7. Yu, S.-J., et al., *Coalescence behaviors of telephone cord buckles in SiAlN_x films*. Surface and Coatings Technology, 2013. **232**: p. 884-890.
8. Chason, E., et al., *Origin of compressive residual stress in polycrystalline thin films*. Phys Rev Lett, 2002. **88**(15): p. 156103.
9. Korsunsky, A.M., et al., *Nanoscale residual stress depth profiling by Focused Ion Beam milling and eigenstrain analysis*. Materials & Design, 2018. **145**: p. 55-64.
10. Jun Young Chung, T.Q.C., Michael J. Fasolka, Hyun Wook Ro, and Christopher M. Stafford, *Quantifying residual stress in nanoscale thin polymer films via surface via wrinkling*. ACS Nano, 2009. **3**: p. 845-852.
11. Wang, H., et al., *Interfacial Residual Stress Relaxation in Perovskite Solar Cells with Improved Stability*. Adv Mater, 2019: p. e1904408.
12. Cao, S.G., et al., *Stress-Induced Cubic-to-Hexagonal Phase Transformation in Perovskite Nanorods*. Nano Lett, 2017. **17**(8): p. 5148-5155.
13. Zhang, Y., W.H. Wang, and A.L. Greer, *Making metallic glasses plastic by control of residual stress*. Nat Mater, 2006. **5**(11): p. 857-60.
14. Gruber, D.P., et al., *Gradients of microstructure, stresses and mechanical properties in a multi-layered diamond thin film revealed by correlative cross-sectional nano-analytics*. Carbon, 2019. **144**: p. 666-674.

15. Yu, S.-J., et al., *Morphological selections and dynamical evolutions of buckling patterns in SiAlN_x films: From straight-sided to telephone cord or bubble structures*. Acta Materialia, 2014. **64**: p. 41-53.
16. Bemporad, E., et al., *A critical comparison between XRD and FIB residual stress measurement techniques in thin films*. Thin Solid Films, 2014. **572**: p. 224-231.
17. Sebastiani, M., et al., *Depth-resolved residual stress analysis of thin coatings by a new FIB-DIC method*. Materials Science and Engineering: A, 2011. **528**(27): p. 7901-7908.
18. Archie, F., et al., *Anisotropic distribution of the micro residual stresses in lath martensite revealed by FIB ring-core milling technique*. Acta Materialia, 2018. **150**: p. 327-338.
19. Withers, P.J. and H.K.D.H. Bhadeshia, *Residual stress. Part 1 – Measurement techniques*. Materials Science and Technology, 2001. **17**(4): p. 355-365.
20. Everaerts, J., et al., *Separating macro- (Type I) and micro- (Type II+III) residual stresses by ring-core FIB-DIC milling and eigenstrain modelling of a plastically bent titanium alloy bar*. Acta Materialia, 2018. **156**: p. 43-51.
21. Mansilla C., M.-M.D., Ocelík V., De Hosson J.T.M., *On the determination of local residual stress gradients by the slit milling method*. J. Mater. Sci. , 2015. **50**(10): p. 3646–3655.
22. Mansilla C., O.V., De Hosson J.T.M., *Local residual stress measurements on nitride layers*. Mater. Sci. Eng. A, 2015. **636**: p. 476–483.
23. Gao, Z., et al., *Comparison of the oxidation behavior of a zirconium nitride coating in water vapor and air at high temperature*. Corrosion Science, 2018. **138**: p. 242-251.
24. Mansilla C., O.V., De Hosson J.T., *A New Methodology to Analyze Instabilities in SEM Imaging*. Microsc. Microanal., 2014. **20**(6): p. 1625–1637.
25. Ma, L.S. and D.W. Lee, *Exact solutions for nonlinear static responses of a shear deformable FGM beam under an in-plane thermal loading*. European Journal of Mechanics - A/Solids, 2012. **31**(1): p. 13-20.
26. Chen, Y., et al., *Effect of platinum addition on oxidation behaviour of γ/γ' nickel aluminide*. Acta Materialia, 2015. **86**: p. 319-330.
27. C. Mennicke, D.R.C., and M. Ruhle, *Stress relaxation in thermally grown alumina scales on heating and cooling FeCrAl and FeCrAlY alloys*. Oxidation of Metals, 2001. **55**: p. 551-569.
28. Gao, Z., et al., *A conformable high temperature nitride coating for Ti alloys*. Acta Materialia, 2020. **189**: p. 274-283.
29. D.H Killpatrick, R.W.B., Acta Metallurgica, 1963. **11**.
30. M. Maeda, M.N., *Interficial reaction between titanium and silicon nitride during solid state diffusion bonding* Trans. JWRI 2001. **30**: p. 59-65.